基于单细胞RNA转录组测序揭示CXCL9:SPP1极化在非酒精性脂肪性肝病进展中的驱动机制

鹿瑶，倪文娟，陈荣翠，王玮

(内蒙古科技大学包头医学院第一附属医院内分泌科，包头 014010)

[摘 要] **目的：**非酒精性脂肪性肝病(non-alcoholic fatty liver disease，NAFLD)是全球流行的慢性肝脏疾病，NAFLD的进展与Kupffer细胞(Kupffer cells，KCs)密切相关。本研究旨在分析NAFLD中KCs的C-X-C趋化因子配体9:分泌型磷蛋白1(C-X-C motif chemokine ligand 9:secreted phosphoprotein 1，CS)极化特征及其与内皮细胞(endothelial cells，ECs)通信的机制。**方法：**通过高通量基因表达数据库(Gene Expression Omnibus，GEO)GSE129516数据集获取3例NAFLD小鼠和3例对照组小鼠肝脏单细胞RNA转录组测序数据，采用Seurat进行数据整合、质量控制、聚类及注释。对KCs与ECs进行亚群划分，并进行基因本体论(Gene Ontology，GO)与京都基因和基因组数据库(Kyoto Encyclopedia of Genes and Genomes，KEGG)富集分析。进一步纳入小鼠肝脏单细胞数据集GSE270583对CS极化进行交叉验证。采用CellChat推断KCs亚群与ECs亚群的细胞间通信网络。将20只雄性C57BL/6J小鼠分为对照组(n=10)和高脂饮食(high-fat diet，HFD)组(n=10)，每周测量小鼠体重，喂养20周时检测小鼠葡萄糖耐量和胰岛素耐量后处死小鼠，留取血清和肝脏进行后续实验。采用苏木精-伊红(hematoxylin and eosin，HE)染色和油红O染色观察肝脏病理学变化，在肝组织中通过免疫荧光染色验证CS极化与M1/M2极化特征。**结果：**共识别出了8类细胞的29个细胞簇。与对照组相比，NAFLD组的KCs比例升高而ECs比例降低。在M1/M2与CS极化下，解析出$CD80^+$ KCs、$CD206^+$ KCs、$S100A4^+$ KCs、分泌型磷蛋白1(secreted phosphoprotein 1，SPP1)$^+$ KCs及C-X-C趋化因子配体9(C-X-C motif chemokine ligand 9，CXCL9)$^+$ KCs等亚群，其中$CD80^+$ KCs与$SPP1^+$ KCs群体显著扩增，其特征基因主要富集于核因子-κB(nuclear factor-kappa B，NF-κB)与肿瘤坏死因子(tumor necrosis factor，TNF)信号通路。过氧化物氧化还原酶(peroxiredoxin，PRDX)3在$CD80^+$ KCs中上调，在$CD206^+$ KCs中下调。ECs可分为$Apoa2^+$ ECs、$PRDX3^+$ ECs及$Col4a1^+$ ECs 3个亚群。在NAFLD组中，$PRDX3^+$ ECs亚群异常活跃，并伴随PRDX1高表达及谷胱甘肽过氧化物酶4(glutathione peroxidase 4，GPX4)的下调。进一步在单细胞数据集GSE270583中进行外部验证，结果显示，$SPP1^+$ KCs与$CXCL9^+$ KCs可明显分离，且NAFLD组中$SPP1^+$ KCs比例升高，支持CS极化在NAFLD中的跨队列可重复性。CellChat分析显示，来自$CD80^+$ KCs和$SPP1^+$ KCs指向$PRDX3^+$ ECs的TNF受体超家族成员1A(TNF receptor superfamily member 1A，TNFRSF1A)信号通路被激活。HFD喂养20周后，小鼠体重较对照组显著增加，并伴发葡萄糖耐量受损及胰岛素敏感性降低(均P<0.05)。HFD组的丙氨酸氨基转移酶(alanine aminotransferase，ALT)、天冬氨酸氨基转移酶(aspartate transferase，AST)、总胆固醇(total cholesterol，TC)、甘油三酯(triglyceride，TG)水平均显著高于对照组(均P<0.05)。HE染色和油红O染色显示，HFD组小鼠肝脏出现明显的排列紊乱、脂质空泡和脂质沉积等变化。免疫荧光染色显示，在肝组织中HFD组PRDX3、CD80表达增多；与对照组相比，HFD组肝脏KCs中SPP1表达升高，而CXCL9表达降低。这些结果与单细胞转录组测序结果一致。**结论：**NAFLD中KCs存在CS极化特征，$SPP1^+$ KCs和$CD80^+$ KCs比例升高，并与$PRDX3^+$ ECs之间的TNF-TNFRSF1A通信增强。HFD小鼠肝组织中SPP1、CXCL9、CD80和PRDX3表达变化与单细胞分析结果基本一致。CS极化可能参与NAFLD肝脏炎症微环境改变的机制，有望为理解NAFLD炎症-纤维化进程提供新的研究方向。

[关键词] 非酒精性脂肪性肝病；单细胞RNA转录组测序；CXCL9:SPP1极化；Kupffer细胞；PRDX3

收稿日期(Date of reception)：2026-01-28

第一作者(First author)：鹿瑶，Email: 17861522779@163.com, ORCID: 0009-0001-5341-4536；倪文娟，Email: 56724025@qq.com, ORCID: 0009-0008-8025-1753

通信作者(Corresponding author)：王玮，主任医师，Email: vvhappy521@163.com, ORCID: 0000-0001-6607-6137

基金项目(Foundation item)：内蒙古自治区自然科学基金(2024MS08018)。This work was supported by the Natural Science Foundation of Inner Mongolia Autonomous Region, China (2024MS08018).

开放获取(Open access)：本文遵循知识共享许可协议，允许第三方用户按照署名-非商业性使用-禁止演绎4.0(CC BY-NC-ND 4.0)的方式，在任何媒介以任何形式复制、传播本作品(https://creativecommons.org/licenses/by-nc-nd/4.0/)。

©Journal of Central South University (Medical Science). All rights reserved.

Single-cell RNA sequencing reveals the driving mechanism of CXCL9:SPP1 polarization in the progression of non-alcoholic fatty liver disease

LU Yao, NI Wenjuan, CHEN Rongcui, WANG Wei

(Department of Endocrinology, First Affiliated Hospital of Baotou Medical College, Inner Mongolia University of Science and Technology, Baotou 014010, China)

ABSTRACT

Objective: Non-alcoholic fatty liver disease (NAFLD) is a globally prevalent chronic liver disease, and its progression is closely associated with Kupffer cells (KCs). This study aims to characterize C-X-C motif chemokine ligand 9∶secreted phosphoprotein 1 (CS) polarization in KCs and investigate its intercellular communication with endothelial cells (ECs) in NAFLD.

Methods: Single-cell RNA sequencing data of liver tissues from 3 NAFLD mice and 3 control mice were obtained from the Gene Expression Omnibus (GEO) dataset GSE129516. Seurat was used for data integration, quality control, clustering, and annotation. KCs and ECs were divided into subgroups, followed by Gene Ontology (GO) and Kyoto Encyclopedia of Genes and Genomes (KEGG) enrichment analyses. A mouse liver single-cell dataset (GSE270583) was further included for cross-validation of CS polarization. CellChat was used to infer intercellular communication networks between KC and EC subgroups. Twenty male C57BL/6J mice were assigned to a control group (n=10) and a high-fat diet (HFD) group (n=10). Body weight was measured weekly. At 20 weeks of feeding, glucose tolerance and insulin tolerance were assessed, after which the mice were sacrificed, and serum and liver tissues were collected for subsequent experiments. Hematoxylin and eosin (HE) staining and Oil Red O staining were used to observe pathological changes in the liver. Immunofluorescence staining of liver tissues was performed to validate the characteristics of CS polarization and M1/M2 polarization.

Results: A total of 29 cell clusters belonging to 8 cell types were identified. Compared with the control group, the proportion of KCs was increased and the proportion of ECs was decreased in the NAFLD group. Under M1/M2 and CS polarization frameworks, subgroups including $CD80^+$ KCs, $CD206^+$ KCs, $S100A4^+$ KCs, secreted phosphoprotein 1 $(SPP1)^+$ KCs, and C-X-C motif chemokine ligand 9 $(CXCL9)^+$ KCs were identified. Among these, $CD80^+$ KCs and $SPP1^+$ KCs were significantly expanded, and their characteristic genes were mainly enriched in nuclear factor-kappa B (NF-κB) and tumor necrosis factor (TNF) signaling pathways. Peroxiredoxin 3 (PRDX3) was upregulated in $CD80^+$ KCs and downregulated in $CD206^+$ KCs. ECs were divided into 3 subgroups: $Apoa2^+$ ECs, $PRDX3^+$ ECs, and $Col4a1^+$ ECs. In the NAFLD group, the $PRDX3^+$ EC subgroup was abnormally active, accompanied by high expression of PRDX1 and downregulation of glutathione peroxidase 4 (GPX4). Further external validation using the single-cell dataset GSE270583

©Journal of Central South University (Medical Science). All rights reserved.

showed that SPP1$^+$ KCs and CXCL9$^+$ KCs could be clearly separated, and the proportion of SPP1$^+$ KCs was increased in the NAFLD group, supporting the cross-cohort reproducibility of CS polarization in NAFLD. CellChat analysis suggested activation of the TNF receptor superfamily member 1A (TNFRSF1A) signaling pathway from CD80$^+$ KCs and SPP1$^+$ KCs to PRDX3$^+$ ECs. After 20-week HFD feeding, mice displayed significant weight gain, impaired glucose tolerance, and reduced insulin sensitivity compared with controls (all $P<0.05$). The levels of alanine aminotransferase (ALT), aspartate transferase (AST), total cholesterol (TC), and triglyceride (TG) were significantly higher in the HFD group than in the control group (all $P<0.05$). HE staining and Oil Red O staining showed marked disordered hepatic architecture, lipid vacuoles, and lipid deposition in the livers of HFD mice. Immunofluorescence staining showed increased expression of PRDX3 and CD80 in liver tissues of the HFD group. Compared with the control group, SPP1 expression was increased, whereas CXCL9 expression was decreased, in hepatic KCs of the HFD group. These results were consistent with the single-cell transcriptome sequencing findings.

Conclusion: KCs in NAFLD exhibit characteristics of CS polarization, with increased proportions of SPP1$^+$ KCs and CD80$^+$ KCs, as well as enhanced TNF-TNFRSF1A communication with PRDX3$^+$ ECs. Changes in the expression of SPP1, CXCL9, CD80, and PRDX3 in the liver tissues of HFD mice were generally consistent with the single-cell analysis results. CS polarization may participate in alterations of the hepatic inflammatory microenvironment in NAFLD and may provide a new research direction for understanding the inflammation-fibrosis progression of NAFLD.

KEY WORDS non-alcoholic fatty liver disease; single-cell RNA sequencing; CXCL9∶SPP1 polarization; Kupffer cells; PRDX3

非酒精性脂肪性肝病(non-alcoholic fatty liver disease，NAFLD)是目前全球最常见的慢性肝病之一，患病率约为25%，其中相当一部分患者会进展为非酒精性脂肪性肝炎(non-alcoholic steatohepatitis，NASH)并进一步发展为肝纤维化、肝硬化甚至肝细胞癌，NAFLD已成为肝移植和肝相关死亡的重要病因之一[1-2]。NAFLD并非单纯脂质沉积所致，而是由代谢紊乱、免疫炎症反应、氧化应激及多种程序性细胞死亡共同驱动的复杂疾病过程。既往研究[3-4]显示，药物因素可通过影响载脂蛋白(apolipoprotein，Apo)A5的分泌诱导肝脏脂质沉积，提示脂蛋白代谢异常是NAFLD发生的重要环节之一；同时，血浆脂质水平与NAFLD及肝酶异常之间也存在密切关联，进一步支持脂质代谢紊乱在NAFLD发生、发展中的核心作用。肝内先天免疫细胞，尤其是Kupffer细胞(Kupffer cells，KCs)，在炎症放大、肝实质损伤及纤维化形成中发挥核心作用[5-6]。

传统的巨噬细胞研究多采用M1(促炎型)/M2(抗炎或修复型)这一经典二元极化模式来解释其功能差异，但随着单细胞转录组测序技术在肝病领域的广泛应用，KCs在体内呈现高度异质性的功能状态可能超出M1/M2分类。在代谢相关脂肪性肝病(metabolic dysfunction-associated steatotic liver disease，MASLD)中，既有来源于卵黄囊的驻留KCs，也有单核细胞来源的浸润性巨噬细胞，二者在空间分布、转录特征和功能上存在显著差异，共同构成复杂的“巨噬细胞景观”[5-7]。因此，有必要在单细胞水平上重新审视巨噬细胞极化模式，以更好地理解NAFLD的炎症-纤维化进展。

在新的功能分型尝试中，以C-X-C趋化因子配体9(C-X-C motif chemokine ligand 9，CXCL9)和分泌型磷蛋白1(secreted phosphoprotein 1，SPP1)为代表的

©Journal of Central South University (Medical Science). All rights reserved.

极化模式受到关注。多项研究[1, 8-9]发现SPP1在NAFLD和NASH的肝组织和外周血中显著升高，与炎症程度和纤维化分期密切相关，是潜在的无创标志物和治疗靶点。CXCL9作为γ干扰素(interferon-gamma，IFN-γ)相关的趋化因子，在炎症微环境中可招募Th1细胞和$CD8^+$ T细胞，参与抗病毒和抗肿瘤免疫，同时在部分代谢性和自身免疫性肝病中也被报道与疾病活动度相关[1, 10]。在肿瘤等疾病领域，以CXCL9高表达和SPP1高表达来界定2类功能不同的巨噬细胞群体，发现CXCL9:SPP1(CS)极化相比传统的M1/M2极化具有更强的预后关联性[11-13]，提示这一新的极化模式可能更好地反映巨噬细胞在炎症、纤维化和免疫调控中的双重角色。

除巨噬细胞外，肝窦内皮细胞(endothelial cells，ECs)是连接血流、肝细胞和免疫细胞的关键界面，在NAFLD的发生、发展中扮演“放大器”和“整合器”的角色。ECs功能障碍可导致窦状隙毛细血管化、局部缺氧、门静脉高压及星状细胞活化，从而推动纤维化进展[2, 14]。

过氧化物氧化还原酶(peroxiredoxin，PRDX)3是定位于线粒体的抗氧化酶，负责清除线粒体源活性氧(reactive oxygen species，ROS)，维持线粒体稳态和细胞生存。已有动物实验[6, 15]证明，调控PRDX3及其上游沉默信息调节因子(sirtuin，SIRT)家族去乙酰化酶可以改善肝脏氧化应激反应，减轻肝炎症和纤维化。还有研究[16]发现，高氧化状态的PRDX3可作为铁死亡的特异性标志，其在酒精性脂肪性肝病和NAFLD模型中显著累积，并与肝细胞死亡和慢性肝损伤程度密切相关。这些结果表明，PRDX3可能一方面通过抗氧化限制ROS累积；另一方面在极端氧化应激下又参与铁死亡，是连接氧化应激与细胞死亡的重要枢纽。然而，目前关于PRDX3在NAFLD KCs极化、ECs损伤及二者中的具体作用仍缺乏系统研究，尚不能从整体上解释其在NAFLD炎症-纤维化进展中的功能。

本研究旨在结合单细胞RNA转录组测序(single-cell RNA sequencing，scRNA-seq)和动物模型，探究NAFLD中KCs CS极化与ECs损伤之间的关系，从而进一步解析NAFLD的免疫发病机制。

1 材料与方法

1.1 伦理声明

本研究已获得内蒙古科技大学包头医学院第一附属医院医学伦理委员会批准(审批号：2024-D026)。

1.2 ScRNA-seq

1.2.1 数据获取及处理

通过基因表达综合数据库(Gene Expression Omnibus，GEO)[17]中的GSE129516数据集获取3例NAFLD小鼠和3例对照小鼠的单细胞转录组数据。另纳入GSE270583小鼠肝脏单细胞数据集用于验证CS极化在独立数据集中的可重复性。单细胞数据的详细质控、整合、降维流程见补充材料(https://doi.org/10.57760/sciencedb.xbyxb.00151)。

1.2.2 数据质控、聚类及细胞注释

采用Seurat v4.1.0对GSE129516数据进行质量控制、标准化、批次校正、降维和聚类分析。细胞类型注释基于Seurat FindAllMarkers函数筛选的差异表达基因，并结合CellMarker 2.0数据库[18]及既往肝脏单细胞转录组研究[19-20]进行综合判定。

1.2.3 单细胞亚群分析与功能富集

提取KCs和ECs后分别进行亚群分析，重新进行降维、聚类和注释。使用FindClusters和RunUMAP函数重新聚类和降维，以识别该细胞群中的亚群。采用R包clusterProfiler[21]对KCs特异性上调基因进行基因本体论(Gene Ontology，GO)与京都基因和基因组数据库(Kyoto Encyclopedia of Genes and Genomes，KEGG)功能富集分析[22-24]，以识别显著富集的生物学功能和信号通路。

1.2.4 独立数据集交叉验证

采用GSE270583作为外部验证队列。根据原始注释提取KCs后，基于发现队列中$SPP1^+$ KCs与$CXCL9^+$ KCs的特征上调基因构建signature，并采用UCell计算每个KC的SPP1和CXCL9极化得分。以SPP1与CXCL9 signature score各自分布的上四分位数作为高分阈值，进行双轴分群：SPP1高/CXCL9低定义为$SPP1^+$ KCs，CXCL9高/SPP1低定义为$CXCL9^+$ KCs，双高定义为Mixed_Doublet，双低定义为Other。随后比较对照组与NAFLD组中不同极化状态的组成比例。

©Journal of Central South University (Medical Science). All rights reserved.

1.2.5 细胞通信网络构建

为进一步探究KCs亚群与ECs亚群之间的通信关系，采用CellChat进行细胞间通信分析。基于R包CellChat v1.6.1推断细胞间的通信关系，CellChat使用质量作用模型，对细胞组的差异表达进行分析和统计测试，在给定的scRNA-seq数据内推断细胞状态特定的信号通信。

1.3 动物实验

1.3.1 动物模型构建

选用4周龄的雄性C57BL/6J小鼠[斯贝福(北京)生物技术有限公司]。所有动物被饲养在12 h/12 h的光/暗循环、温度为22~24 ℃、湿度为50%~60%的环境中，可自由获取水和食物。

将20只小鼠分为2组：对照组、高脂饮食(high-fat diet，HFD)组，每组10只。其中对照组给予普通饲粮[斯贝福(北京)生物技术有限公司，维持饲料]喂养，HFD组给予高脂饲粮[小黍有泰(北京)生物科技有限公司，D12492]，喂养20周后，建立NAFLD模型。每周测量1次体重，在第20周间隔5 d进行腹腔注射葡萄糖耐量试验(intraperitoneal glucose tolerance test，IPGTT)和胰岛素耐量试验(intraperitoneal insulin tolerance test，IPITT)，分别于空腹12 h和6 h后测定基线血糖，之后腹腔注射葡萄糖(2 g/kg)或胰岛素(1 U/kg)，并在注射后15、30、60、90和120 min经尾静脉采血，采用葡萄糖氧化酶法血糖仪(三诺生物传感股份有限公司)测定血糖水平。通过异氟烷麻醉后颈椎脱臼处死所有小鼠，留取小鼠肝脏和血清进行后续实验。

1.3.2 生化检测

使用全自动生化分析仪Indiko(美国赛默飞世尔公司)对小鼠血清样本进行天冬氨酸氨基转移酶(aspartate transferase，AST)、丙氨酸氨基转移酶(alanine aminotransferase，ALT)、总胆固醇(total cholesterol，TC)、甘油三酯(triglyceride，TG)检测，根据校准曲线和反应吸光度变化自动计算出各样本指标的浓度。

1.3.3 病理学染色

肝组织取材后用4%多聚甲醛固定24 h以上，石蜡包埋切片后进行苏木精-伊红(hematoxylin and eosin，HE)染色；另取新鲜肝组织制备冰冻切片，并进行油红O染色。染色后使用光学显微镜进行观察并拍照。

1.3.4 免疫荧光染色

组织取材后用4%多聚甲醛固定24 h以上，石蜡包埋切片后分别与相应一抗于4 ℃孵育过夜。次日加入相应荧光标记二抗，于室温避光孵育50 min。随后用4’, 6-二脒基-2-苯基吲哚(4’, 6-diamidino-2-phenylindole，DAPI)复染细胞核10 min。图像采集使用尼康共聚焦显微镜完成。所用一抗、二抗的厂家、货号及稀释比例见附表1(https://doi.org/10.57760/sciencedb.xbyxb.00151)。

1.4 统计学处理

采用GraphPad Prism 10.1.2软件进行统计学分析。数据以均数±标准差表示。体重变化及在IPGTT、IPITT过程中不同时间点的动态变化采用双因素重复测量方差分析；曲线下面积(area under the curve，AUC)、血清生化指标及免疫荧光半定量结果等组间比较采用独立样本t检验。所有检验均为双侧检验，P<0.05为差异有统计学意义。

2 结 果

2.1 单细胞聚类与细胞类型注释

对GSE129516数据进行质量控制、标准化及降维分析后，共纳入33 062个细胞、19 349个基因用于后续分析。高变基因筛选及主成分分析显示数据质量良好，且各样本间未见明显批次分离(附图1，https://doi.org/10.57760/sciencedb.xbyxb.00151)。

通过UMAP降维分析得到29个细胞群，结合CellMarker 2.0数据库及经典差异基因表达模式进行细胞类型注释，相关聚类结果及基因表达情况见附图2A和2B(https://doi.org/10.57760/sciencedb.xbyxb.00151)。共鉴定出8类主要细胞类型：胆管细胞、B细胞、树突状细胞、ECs、肝星状细胞、肝细胞、KCs及T/自然杀伤(natural killer，NK)细胞(图1A)。其中KCs比例在NAFLD样本中明显增加，而ECs显著减少(图1B)。

2.2 KCs亚群分析及CS极化的独立数据集验证

在NAFLD中，基于经典M1/M2极化标志物及

©Journal of Central South University (Medical Science). All rights reserved.

CS极化对KCs进行亚群划分(图2A)。在M1/M2极化下，鉴定出3个主要亚群：CD80$^+$ KCs、CD206$^+$ KCs和S100A4$^+$ KCs(图2B)。其中，CD206$^+$ KCs表达经典的M2标志物(如CD206、MRC1)。S100A4$^+$ KCs的典型M1/M2标志物表达较低，因此被定义为S100A4$^+$“M0样”KCs(附图2C，https://doi.org/10.57760/sciencedb.xbyxb.00151)。促炎性的CD80$^+$ KCs亚群在NAFLD中显著扩增(图2D)。PRDX3在CD80$^+$ KCs中表达升高，而在CD206$^+$ KCs中表达降低。对CD80$^+$ KCs中特异性上调的基因进行GO和KEGG富集分析，结果显示炎症相关通路显著富集，其中核因子-κB(nuclear factor-kappa B，NF-κB)信号通路与肿瘤坏死因子(tumor necrosis factor，TNF)信号通路的富集得分最高(附图3，https://doi.org/10.57760/sciencedb.xbyxb.00151)。

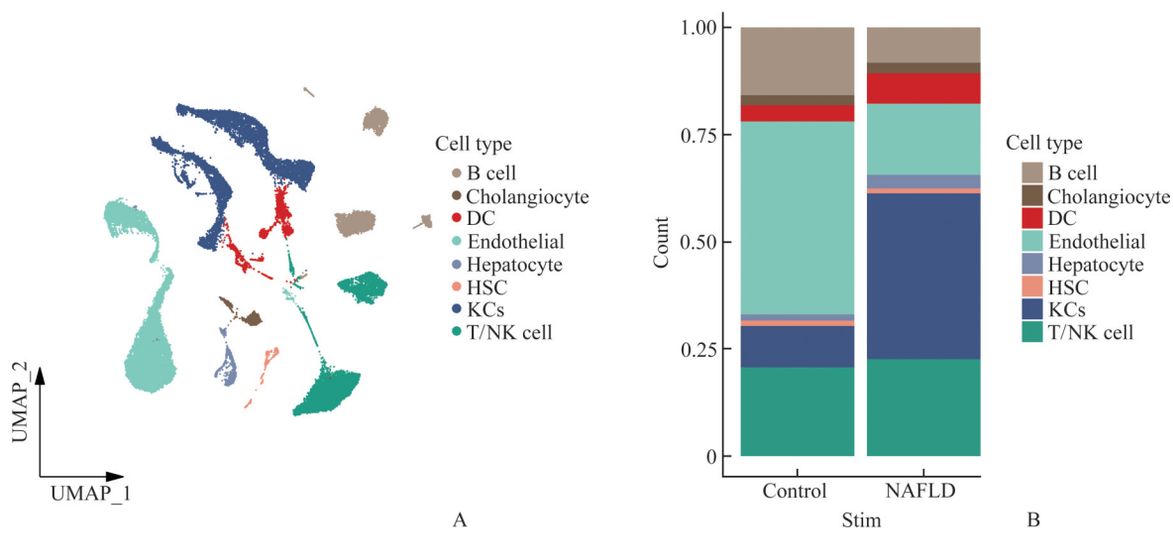


图1　单细胞图谱揭示主要细胞类型及组成变化

Figure 1　Single-cell atlas reveals major cell types and compositional changes

A: UMAP plot of annotated cell types. B: Proportions of major cell types in the control and NAFLD groups. DC: Dendritic cell; HSC: Hepatic stellate cell; NAFLD: Non-alcoholic fatty liver disease; KCs: Kupffer cells; NK: Natural killer.

在CS极化下，同样解析出3个主要亚群：SPP1$^+$ KCs、CXCL9$^+$ KCs和Igha$^+$ KCs(图2C)。CXCL9$^+$ KCs表达经典的CXCL9标志物；而Igha$^+$ KCs的CS标志物表达较低，被定义为未极化的Igha$^+$ KCs状态(附图2D，https://doi.org/10.57760/sciencedb.xbyxb.00151)。值得注意的是，SPP1$^+$ KCs在NAFLD中同样显著扩增(图2E)，并表达多种促炎介质。对SPP1$^+$ KCs中特异性上调基因的GO和KEGG分析显示其特征基因同样富集于NF-κB与TNF等炎症相关通路(附图3，https://doi.org/10.57760/sciencedb.xbyxb.00151)。

为评估CS极化在独立队列中的可重复性，本研究进一步纳入GSE270583小鼠肝脏scRNA-seq数据进行验证(附图4A、4B，https://doi.org/10.57760/sciencedb.xbyxb.00151)。提取其中KCs后，基于发现队列中SPP1$^+$ KCs与CXCL9$^+$ KCs的特征基因构建UCell评分，结果显示，外部队列中的KCs可依据SPP1/CXCL9双轴评分分为不同极化状态，其中SPP1$^+$ KCs与CXCL9$^+$ KCs呈明显分离(图2F)；同时，与对照组相比，NAFLD组中SPP1$^+$ KCs比例升高，提示CS极化在独立小鼠NAFLD单细胞数据中具有较好的跨队列稳定性(图2G)。

2.3　ECs亚群分析及KCs-ECs间细胞通信

提取ECs并进一步注释后，共获得3个亚群：Apoa2$^+$ ECs、PRDX3$^+$ ECs和Col4a1$^+$ ECs(图3A、3B)。各ECs亚群代表性差异基因的表达模式见附图2E(https://doi.org/10.57760/sciencedb.xbyxb.00151)。比例分析显示，NAFLD中PRDX3$^+$ ECs亚群异常活跃(图3C)。该亚群高表达氧化应激相关基因*PRDX1*，

©Journal of Central South University (Medical Science). All rights reserved.

同时谷胱甘肽过氧化物酶4(glutathione peroxidase 4，GPX4)显著下调，提示其可能处于氧化应激及潜在铁死亡相关状态。

细胞间通信分析结果显示，KCs与ECs不同亚群之间存在差异性通信强度和通信数量(图3D、3E)。进一步的配体-受体分析提示，$CD80^+$/$SPP1^+$ KCs与$PRDX3^+$ ECs之间的TNF受体超家族成员1A(TNF receptor superfamily member 1A，TNFRSF1A)信号通路被激活(图3F、3G)。

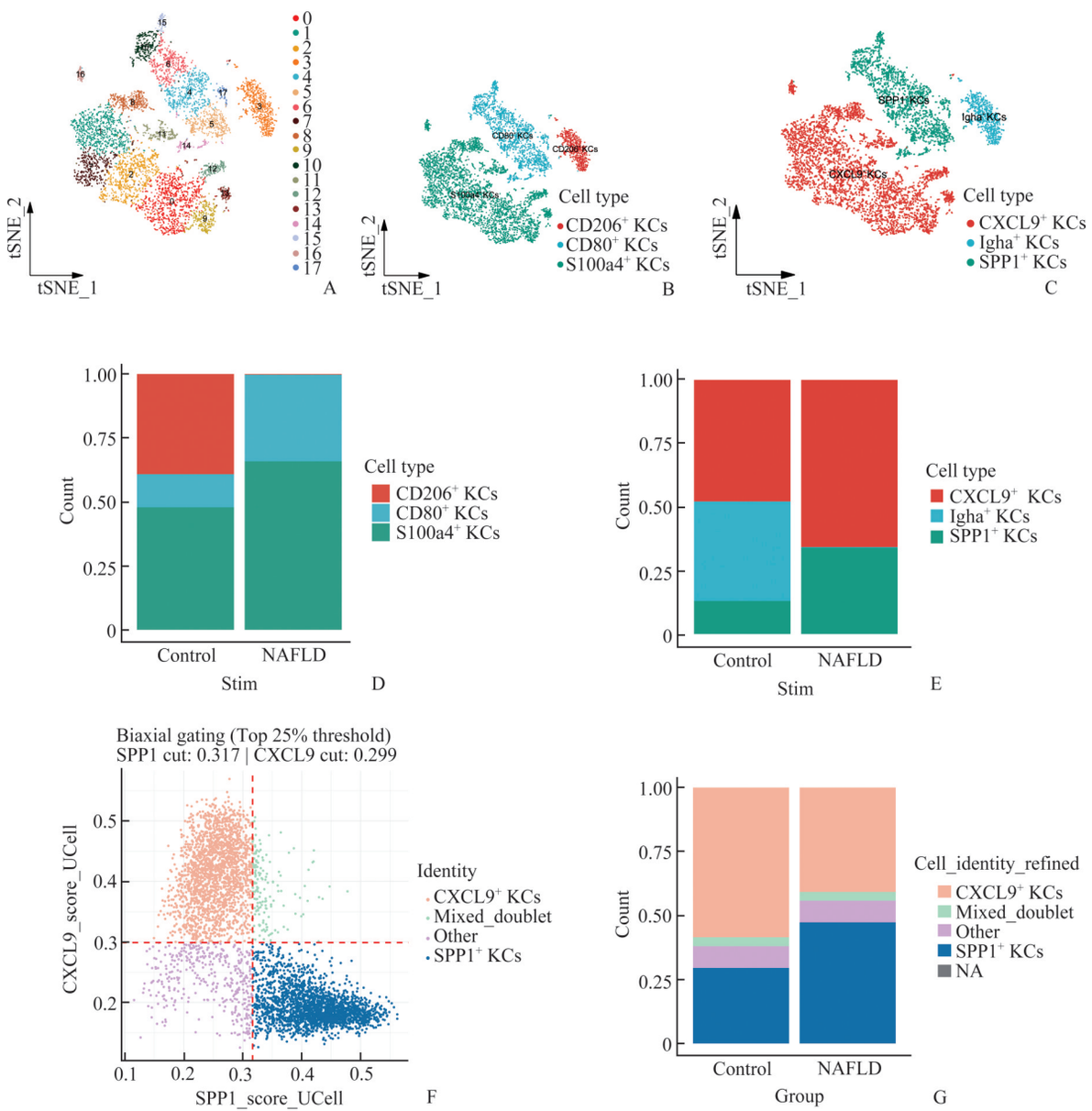


图2 KCs亚群分析及CS极化的独立数据集验证

Figure 2 KCs subcluster analysis and validation of CS polarization in an independent dataset

A: tSNE plot of KCs subclusters. B: Annotation of KCs subclusters under the M1/M2 polarization framework. C: Annotation of KCs subclusters under the CS polarization framework. D: Proportions of KCs subclusters under the M1/M2 polarization framework. E: Proportions of KCs subclusters under the CS polarization framework. F: Biaxial gating plot of SPP1/CXCL9 scores in KCs. G: Proportions of different CS polarization states in KCs from the control and NAFLD groups. CXCL9: C-X-C motif chemokine ligand 9; SPP1: Secreted phosphoprotein 1; CS: CXCL9:SPP1; tSNE: t-Distributed stochastic neighbor embedding.

©Journal of Central South University (Medical Science). All rights reserved.

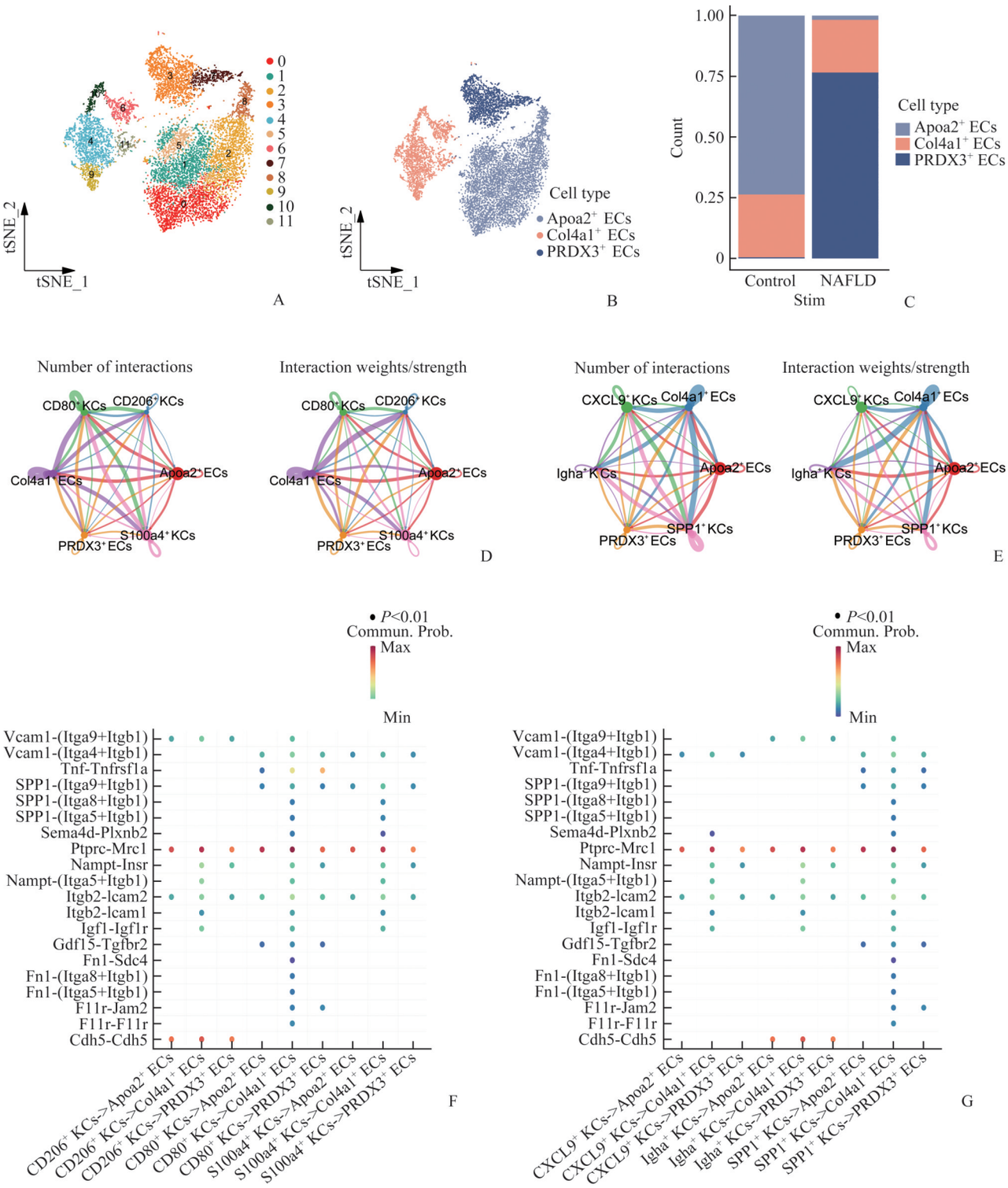


图3　ECs亚群改变及KCs-ECs间细胞通信

Figure 3　ECs subcluster alterations and intercellular communication between KCs and ECs

A: tSNE plot of ECs subclusters. B: Annotated ECs subclusters. C: Proportions of EC subclusters. D and E: Number and strength of interactions between KC and EC subclusters under the M1/M2 (D) and CS (E) polarization framework. F and G: CellChat bubble plot showing ligand-receptor interactions between KC and EC subclusters under the M1/M2 (F) and CS (G) polarization framework. ECs: Endothelial cells; PRDX3: Peroxiredoxin 3.

©Journal of Central South University (Medical Science). All rights reserved.

2.4 CS极化与M1/M2极化在NAFLD小鼠模型中的表达特征

高脂喂养20周后，HFD组小鼠的体重相较于对照组明显升高(图4A)。IPGTT结果显示，与对照组相比，HFD组小鼠在0、15、30和60 min的血糖水平均显著升高，且AUC明显增加(均P<0.05，图4B)，提示空腹血糖升高及葡萄糖耐量受损。IPITT结果显示，HFD组小鼠在90、120 min的血糖水平均显著升高，且AUC明显增加(均P<0.05，图4C)，提示胰岛素敏感性下降。HFD组小鼠血清的ALT、AST及TC、TG水平均较对照组升高(均P<0.05，图4D~4G)，提示其出现肝损伤及脂代谢异常。与对照组相比，HE染色结果显示，HFD组小鼠肝脏出现了明显的脂质空泡和肝细胞排列紊乱，油红O染色显示出HFD组存在显著的脂质蓄积(图5A)。以上特征提示成功构建小鼠NAFLD模型。

免疫荧光结果显示，在肝组织中与对照组相比，HFD组CD80表达显著增加，而CD206表达下降，同时PRDX3表达水平升高(图5B)。相较于对照组，HFD组肝脏KCs[集落刺激因子1受体(colony-stimulating factor 1 receptor，CSF1R)表达阳性]的SPP1表达增加，CXCL9表达下降(图5C)，这与scRNA-seq结果一致。

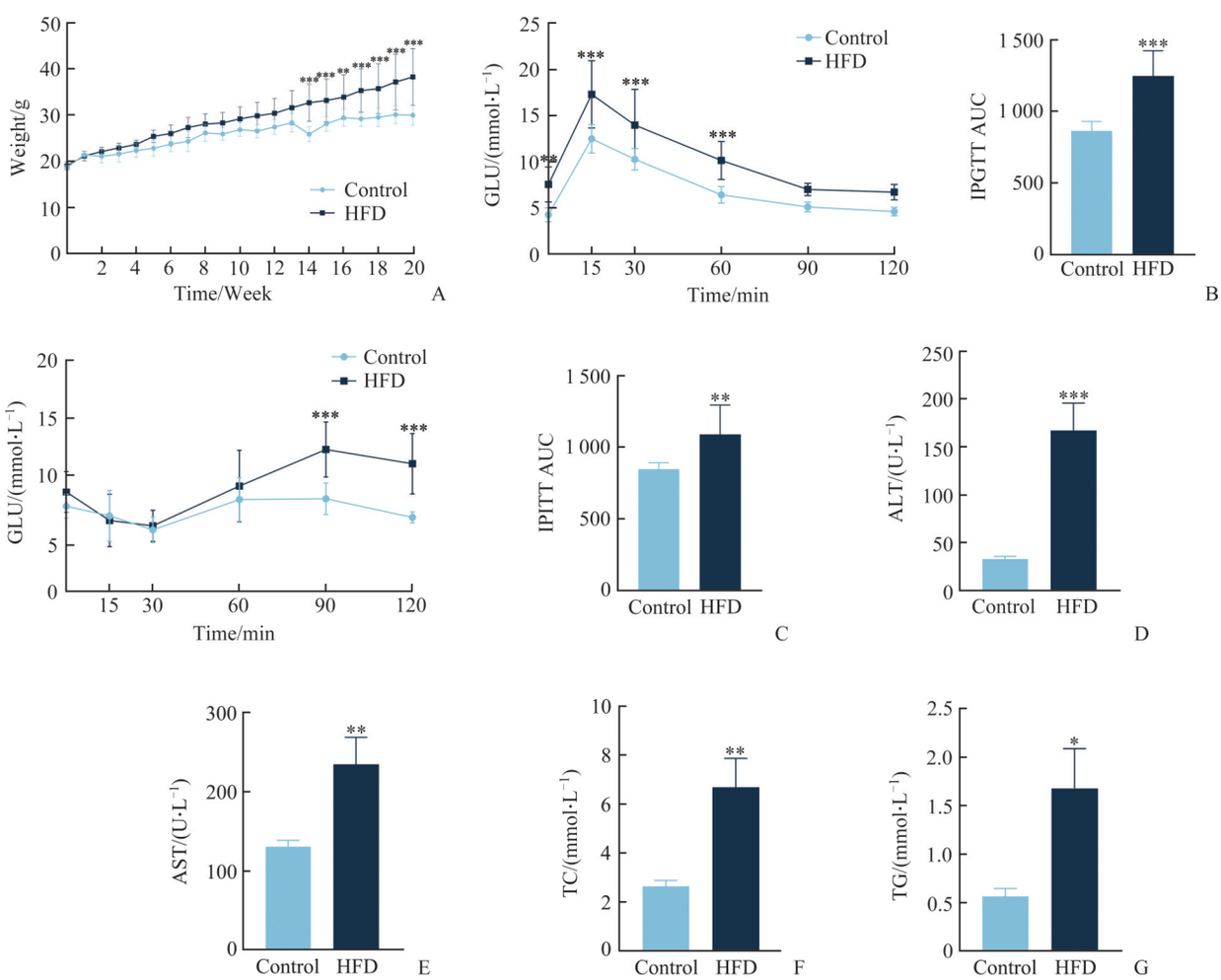


图4 小鼠模型中的糖脂代谢水平变化

Figure 4 Changes in glucose and lipid metabolism in the mouse model

A: Body weight changes in mice after 20 weeks of feeding. B: IPGTT result and its AUC. C: IPITT result and its AUC. D−G: Serum ALT (D), AST (E), TC (F), and TG (G) levels in mice. n=10. *P<0.05, **P<0.01, ***P<0.001 vs the control group. HFD: High-fat diet; IPGTT: Intraperitoneal glucose tolerance test; IPITT: Intraperitoneal insulin tolerance test; GLU: Glucose; AST: Aspartate transferase; ALT: Alanine aminotransferase; TC: Total cholesterol; TG: Triglyceride; AUC: Area under the curve.

©Journal of Central South University (Medical Science). All rights reserved.

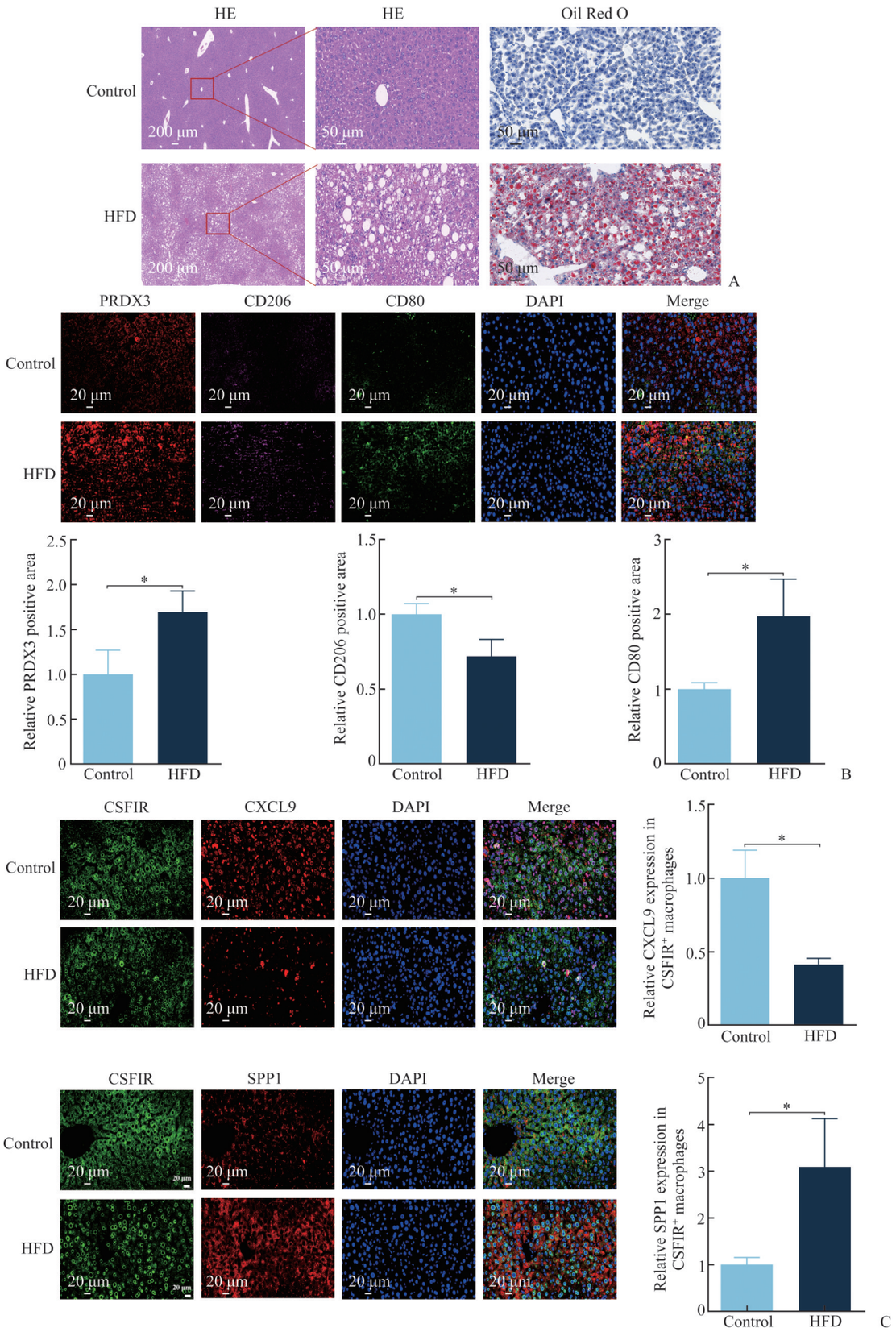


图5　小鼠肝脏病理形态学及免疫荧光染色

Figure 5　Hepatic histopathology and immunofluorescence staining in mice

A: HE staining and Oil Red O staining of liver sections. B: Immunofluorescence staining and semi-quantitative analysis of CD80, CD206, and PRDX3 in liver tissues. C: Immunofluorescence staining and semi-quantitative analysis of CXCL9 and SPP1 in hepatic KCs (CSF1R-positive). *P<0.05. HE: Hematoxylin and eosin; DAPI: 4’,6-diamidino-2-phenylindole; CSF1R: Colony-stimulating factor 1 receptor.

©Journal of Central South University (Medical Science). All rights reserved.

3 讨 论

本研究结合scRNA-seq和动物实验，发现NAFLD中KCs存在区别于传统M1/M2模式的CS极化特征，并发现PRDX3可能参与KCs极化及其与ECs的异常通信。

传统观点中，NAFLD进展过程中KCs的“活化失衡”被认为与疾病严重程度相关：M1型KCs增多常伴随更重的肝炎症和胰岛素抵抗，而M2型KCs则通过释放抗炎介质及与星状细胞互作影响纤维化进程。然而M2的作用机制并非统一，如M2a、M2d等亚型同样能促进肝星状细胞激活和胶原沉积；相反，M1型KCs在特定情况下也参与免疫监视和抗肿瘤[25]。仅用M1/M2 2类难以概括KCs在NAFLD中的多重作用[26-28]。利用CS极化对KCs进行重新分类，CXCL9高表达的KCs具有强烈的促炎特征，可分泌CXCL9等趋化因子吸引Th1淋巴细胞和CTL浸润肝组织，加剧局部炎症反应；而SPP1高表达的KCs富集于纤维化病灶区域，是促进肝纤维组织重塑的关键驱动者[11, 27]。研究[27, 29]表明，在NASH肝脏中出现了一类“脂质相关巨噬细胞”，其高度表达SPP1，与纤维化进展显著相关。本研究结果同样显示SPP1$^+$ KCs在NAFLD小鼠中富集。这些KCs表现出代谢调节的特征而非经典的促炎性质[29]，再次说明简单的M1/M2框架不足以描述其功能。相比之下，CS极化能够同时捕捉KCs由CXCL9介导的促炎潜能和由SPP1介导的促纤维化潜能，提供了对NAFLD免疫病理机制更全面的解释视角。另外在肿瘤等疾病中也观察到CS极化状态比M1/M2分类更具预后价值[12, 30]，提示在慢性肝病中这一模式同样可能具有重要的指示作用。因此，相对于传统的M1/M2分类，CS极化可能更能反映NAFLD中KCs功能状态的连续变化及其对疾病进程的影响。

本研究发现，PRDX3在肝脏KCs极化和ECs损伤中可能发挥作用。首先，就巨噬细胞极化而言，PRDX3作为线粒体抗氧化体系的重要组成部分，影响巨噬细胞的代谢状态和功能表型[31-35]。在脓毒症相关肺损伤模型中，PRDX3表达降低会加剧线粒体功能紊乱和促炎倾向，使巨噬细胞更易极化为M1表型，而过表达PRDX3则促进巨噬细胞由M1向M2表型转变并恢复线粒体氧代谢功能[31]。其次，就内皮细胞功能而言，PRDX3可能对维持肝脏微循环的完整性发挥重要作用。在NAFLD中，持续的炎症刺激会通过TNF受体1(TNF receptor 1，TNFR1)作用于ECs，诱发ECs产生大量ROS并降低一氧化氮生物利用度，导致ECs功能障碍和毛细血管化[36-37]。PRDX3在ECs中的高表达可能是对抗氧化应激的代偿机制。研究[38]表明，通过上调线粒体脱乙酰酶SIRT3提高PRDX3活性可以减轻缺血/再灌注所致的内皮线粒体氧化损伤。程序性细胞死亡是NAFLD肝细胞损伤和炎症放大的重要机制。除细胞凋亡和焦亡外，铁死亡作为一种由过量脂质过氧化驱动的程序性细胞死亡形式，在NAFLD等疾病中也逐渐受到关注[39-41]。研究[16]鉴定出PRDX3的高氧化形式是铁死亡的特异标志，当细胞发生铁死亡时，大量线粒体脂质过氧化物会使PRDX3过度氧化，从活性形式转变为失活的高氧化形式。因此，在NAFLD的炎症环境中，PRDX3$^+$ ECs亚群的出现可能代表着ECs对抗氧化应激的自我保护。本研究基于scRNA-seq数据观察到PRDX3$^+$ ECs伴随GPX4下调及部分铁死亡相关基因表达变化，但尚未结合功能性证据对内皮细胞铁死亡进行验证，其确切机制仍有待进一步研究。

在NAFLD的免疫微环境中，SPP1$^+$ KCs并非孤立存在，它们通过分泌TNF-α等炎症介质，与周围细胞形成高度交互的网络。大量表达TNF-α的KCs可以激活紧邻的内皮细胞上的TNFR1，触发内皮细胞内的NF-κB等炎症通路和氧化应激反应，造成ECs功能障碍[42-43]。这种KCs-ECs轴在NAFLD进展中具有双重有害作用：一方面，ECs在TNF刺激下分泌趋化因子和黏附分子，促进更多单核细胞和炎症细胞浸润肝脏，从而放大炎症规模[44]；另一方面，受TNF影响的ECs丧失原有的调节血流和维护结构的功能，出现毛细血管化和局部缺氧，结果使肝星状细胞更容易被激活并沉积胶原，从而加速纤维化[45-48]。本研究结果表明，PRDX3$^+$ ECs亚群可能代表TNF相关氧化应激环境下的一类应激反应性ECs状态。临床前研究[44]显示，抑制TNFR1可减轻NAFLD小鼠的肝脂肪变、肝细胞损伤和纤维化。已有综述[49]进一步总结了TNF-α与TNFR信号在NASH进展及靶向治疗中的作用。本研究结果与这些证据相符，即KCs-ECs间通过TNF-TNFR1途径的异常通信，可能是NAFLD由简单脂肪变性向活动性肝炎和纤维化恶化的驱动力之一。

综上所述，本研究通过单细胞转录组学揭示了一种区别于传统M1/M2极化的CS极化，可作为对经典巨噬细胞极化理论的补充。CS极化状态体现了KCs由CXCL9介导促炎和由SPP1介导促纤维化的双重功能，能够更全面地解释NAFLD中炎症到纤维化的病理进程。线粒体抗氧化酶PRDX3在KCs极化及KCs-ECs炎症信号轴中可能发挥关键调控作用，PRDX3可能通过影响细胞氧化应激状态参与KCs极化及ECs异常改变，但其具体调控机制仍需进一步功

©Journal of Central South University (Medical Science). All rights reserved.

能实验验证。以上发现拓展了对NAFLD免疫病理机制的认识，并有望为理解NAFLD炎症-纤维化进程提供新的研究方向。

作者贡献声明：鹿瑶　研究实施，数据采集与分析，论文撰写与修改；倪文娟　数据分析，论文修改；陈荣翠　数据采集与分析；王玮　研究设计与构思，论文审查与修订。所有作者阅读并同意最终的文本。

利益冲突声明：作者声称无任何利益冲突。

参考文献

[1] Wang W, Liu X, Wei P, et al. *SPP1* and *CXCL9* promote non-alcoholic steatohepatitis progression based on bioinformatics analysis and experimental studies[J]. Front Med, 2022, 9: 862278. https://doi.org/10.3389/fmed.2022.862278.

[2] Wallace SJ, Tacke F, Schwabe RF, et al. Understanding the cellular interactome of non-alcoholic fatty liver disease[J]. JHEP Rep, 2022, 4(8): 100524. https://doi.org/10.1016/j.jhepr.2022.100524.

[3] 李蓉, 朱文强, 黄飘飘, 等. 奥氮平通过抑制载脂蛋白A5分泌导致非酒精性脂肪性肝病[J]. 中南大学学报(医学版), 2022, 47(6): 730-738. https://doi.org/10.11817/j.issn.1672-7347.2022.210269.
LI Rong, ZHU Wenqiang, HUANG Piaopiao, et al. Olanzapine causes non-alcoholic fatty liver disease via inhibiting the secretion of apolipoprotein A5[J]. Journal of Central South University. Medical Science, 2022, 47(6): 730-738. https://doi.org/10.11817/j.issn.1672-7347.2022.210269.

[4] 刘志飞, 毕亚茹, 孙成林, 等. 血浆脂质与非酒精性脂肪性肝病及肝酶之间因果关系的孟德尔随机化分析[J]. 吉林大学学报(医学版), 2026, 52(1): 219-227. https://doi.org/10.13481/j.1671-587X.20260123.
LIU Zhifei, BI Yaru, SUN Chenglin, et al. Mendelian randomization analysis on causal association between plasma lipids with nonalcoholic fatty liver disease and liver enzymes [J]. Journal of Jilin University. Medicine Edition, 2026, 52(1): 219-227. https://doi.org/10.13481/j.1671-587X.20260123.

[5] De Ponti FF, Liu Z, Scott CL. Understanding the complex macrophage landscape in MASLD[J]. JHEP Rep, 2024, 6(11): 101196. https://doi.org/10.1016/j.jhepr.2024.101196.

[6] Li W, Chang N, Li L. Heterogeneity and function of kupffer cells in liver injury[J]. Front Immunol, 2022, 13: 940867. https://doi.org/10.3389/fimmu.2022.940867.

[7] Ahamed F, Eppler N, Jones E, et al. Understanding macrophage complexity in metabolic dysfunction-associated steatotic liver disease: transitioning from the M1/M2 paradigm to spatial dynamics[J]. Livers, 2024, 4(3): 455-478. https://doi.org/10.3390/livers4030033.

[8] Kriss M, Golden-Mason L, Kaplan J, et al. Increased hepatic and circulating chemokine and osteopontin expression occurs early in human NAFLD development[J/OL]. PloS One, 2020, 15(7): e0236353[2026-02-01]. https://doi. org/10.1371/journal.pone.0236353.

[9] Zheng Y, Xiong Z, Zhao L, et al. The role of SPP1 in MASLD pathogenesis: Therapeutic insights into ursolic acid's mechanisms of action: Correspondence to editorial on "Ursolic acid targets secreted phosphoprotein 1 to regulate Th17 cells against metabolic dysfunction-associated steatotic liver disease" [J]. Clin Mol Hepatol, 2024, 30(4): 1019-1022. https://doi.org/10.3350/cmh.2024.0471.

[10] Wu X, Yuan C, Pan J, et al. CXCL9, IL2RB, and SPP1, potential diagnostic biomarkers in the co-morbidity pattern of atherosclerosis and non-alcoholic steatohepatitis[J]. Sci Rep, 2024, 14(1): 16364. https://doi.org/10.1038/s41598-024-66287-4.

[11] Bill R, Wirapati P, Messemaker M, et al. *CXCL9: SPP1* macrophage polarity identifies a network of cellular programs that control human cancers[J]. Science, 2023, 381(6657): 515-524. https://doi.org/10.1126/science.ade2292.

[12] Su X, Liang C, Chen R, et al. Deciphering tumor microenvironment: CXCL9 and SPP1 as crucial determinants of tumor-associated macrophage polarity and prognostic indicators[J]. Mol Cancer, 2024, 23(1): 13. https://doi.org/10.1186/s12943-023-01931-7.

[13] Palma A. The landscape of SPP1+ macrophages across tissues and diseases: a comprehensive review[J]. Immunology, 2025, 176(2): 179-196. https://doi.org/10.1111/imm.13952.

[14] Yin J, Xu X, Guo Y, et al. Repair and regeneration: ferroptosis in the process of remodeling and fibrosis in impaired organs [J]. Cell Death Discov, 2024, 10(1): 424. https://doi.org/10.1038/s41420-024-02181-2.

[15] Yu Q, Yang D, Ran B, et al. SIRT4-mediated deacetylation of PRDX3 attenuates liver ischemia reperfusion injury by suppressing ferroptosis[J]. Int J Biol Sci, 2025, 21(10): 4663-4682. https://doi.org/10.7150/ijbs.114510.

[16] Cui S, Ghai A, Deng Y, et al. Identification of hyperoxidized PRDX3 as a ferroptosis marker reveals ferroptotic damage in chronic liver diseases[J]. Mol Cell, 2023, 83(21): 3931-3939. https://doi.org/10.1016/j.molcel.2023.09.025.

[17] Clough E, Barrett T, Wilhite SE, et al. NCBI GEO archive for gene expression and epigenomics data sets: 23-year update[J]. Nucleic Acids Res, 2024, 52(D1): D138-D144. https://doi.org/10.1093/nar/gkad965.

[18] Hu C, Li T, Xu Y, et al. CellMarker 2.0: an updated database of manually curated cell markers in human/mouse and web tools based on scRNA-seq data[J]. Nucleic Acids Res, 2023, 51(D1): D870-D876. https://doi.org/10.1093/nar/gkac947.

[19] Xiong X, Kuang H, Ansari S, et al. Landscape of intercellular crosstalk in healthy and NASH liver revealed by single-cell secretome gene analysis[J]. Mol Cell, 2019, 75(3): 644-660. https://doi.org/10.1016/j.molcel.2019.07.028.

[20] MacParland SA, Liu JC, Ma XZ, et al. Single cell RNA sequencing of human liver reveals distinct intrahepatic macrophage populations[J]. Nat Commun, 2018, 9(1): 4383. https://doi.org/10.1038/s41467-018-06318-7.

[21] Yu G, Wang L, Han Y, et al. clusterProfiler: an R package for comparing biological themes among gene clusters[J]. OMICS A J Integr Biol, 2012, 16(5): 284-287. https://doi.org/10.1089/omi.2011.0118.

[22] Kanehisa M, Furumichi M, Sato Y, et al. KEGG: biological systems database as a model of the real world[J]. Nucleic Acids Res, 2025, 53(D1): D672-D677. https://doi.org/10.1093/nar/gkae909.

[23] Kanehisa M. Toward understanding the origin and evolution of

©Journal of Central South University (Medical Science). All rights reserved.

cellular organisms[J]. Protein Sci, 2019, 28(11): 1947-1951. https://doi.org/10.1002/pro.3715.

[24] Kanehisa M, Goto S. KEGG Kyoto encyclopedia of genes and genomes[J]. Nucleic Acids Res, 2000, 28(1): 27-30. https://doi.org/10.1093/nar/28.1.27.

[25] Kohlhepp MS, Liu HY, Tacke F, et al. The contradictory roles of macrophages in non-alcoholic fatty liver disease and primary liver cancer—Challenges and opportunities[J]. Front Mol Biosci, 2023, 10: 1129831. https://doi.org/10.3389/fmolb.2023.1129831.

[26] Vonderlin J, Chavakis T, Sieweke M, et al. The multifaceted roles of macrophages in NAFLD pathogenesis[J]. Cell Mol Gastroenterol Hepatol, 2023, 15(6): 1311-1324. https://doi.org/10.1016/j.jcmgh.2023.03.002.

[27] Remmerie A, Martens L, Thoné T, et al. Osteopontin expression identifies a subset of recruited macrophages distinct from kupffer cells in the fatty liver[J]. Immunity, 2020, 53(3): 641-657. https://doi.org/10.1016/j.immuni.2020.08.004.

[28] Parthasarathy G, Malhi H. Macrophage heterogeneity in NASH: more than just nomenclature[J]. Hepatology, 2021, 74(1): 515-518. https://doi.org/10.1002/hep.31790.

[29] Han H, Ge X, Komakula SSB, et al. Macrophage-derived osteopontin (SPP1) protects from nonalcoholic steatohepatitis [J]. Gastroenterology, 2023, 165(1): 201-217. https://doi.org/10.1053/j.gastro.2023.03.228.

[30] Xu L, Chen Y, Liu L, et al. Tumor-associated macrophage subtypes on cancer immunity along with prognostic analysis and SPP1-mediated interactions between tumor cells and macrophages[J/OL]. PloS Genet, 2024, 20(4): e1011235[2026-02-01]. https://doi.org/10.1371/journal.pgen.1011235.

[31] Huang W, Wang L, Huang Z, et al. Peroxiredoxin 3 has a crucial role in the macrophage polarization by regulating mitochondrial homeostasis[J]. Respir Res, 2024, 25(1): 110. https://doi.org/10.1186/s12931-024-02739-9.

[32] Jeong SJ, Park JG, Oh GT. Peroxiredoxins as potential targets for cardiovascular disease[J]. Antioxidants (Basel), 2021, 10(8): 1244. https://doi.org/10.3390/antiox10081244.

[33] Manoharan RR, Prasad A, Pospíšil P, et al. ROS signaling in innate immunity via oxidative protein modifications[J]. Front Immunol, 2024, 15: 1359600. https://doi.org/10.3389/fimmu.2024.1359600.

[34] Canton M, Sánchez-Rodríguez R, Spera I, et al. Reactive oxygen species in macrophages: sources and targets[J]. Front Immunol, 2021, 12: 734229. https://doi.org/10.3389/fimmu.2021.734229.

[35] Lee S, Wi SM, Min Y, et al. Peroxiredoxin-3 is involved in bactericidal activity through the regulation of mitochondrial reactive oxygen species[J]. Immune Netw, 2016, 16(6): 373-380. https://doi.org/10.4110/in.2016.16.6.373.

[36] Zhang H, Park Y, Wu J, et al. Role of TNF-α in vascular dysfunction[J]. Clin Sci, 2009, 116(3): 219-230. https://doi.org/10.1042/cs20080196.

[37] Lafoz E, Ruart M, Anton A, et al. The endothelium as a driver of liver fibrosis and regeneration[J]. Cells, 2020, 9(4): 929. https://doi.org/10.3390/cells9040929.

[38] Wang Z, Sun R, Wang G, et al. SIRT3-mediated deacetylation of PRDX3 alleviates mitochondrial oxidative damage and apoptosis induced by intestinal ischemia/reperfusion injury[J]. Redox Biol, 2020, 28: 101343. https://doi.org/10.1016/j.redox.2019.101343.

[39] Dixon SJ, Olzmann JA. The cell biology of ferroptosis[J]. Nat Rev Mol Cell Biol, 2024, 25(6): 424-442. https://doi.org/10.1038/s41580-024-00703-5.

[40] Jiang X, Stockwell BR, Conrad M. Ferroptosis: mechanisms, biology and role in disease[J]. Nat Rev Mol Cell Biol, 2021, 22(4): 266-282. https://doi.org/10.1038/s41580-020-00324-8.

[41] 曹赛颖, 龙毅, 杨丽娜. Caspase-3调控非酒精性脂肪性肝病细胞焦亡和凋亡的研究进展[J]. 中南大学学报(医学版), 2025, 50(6): 1060-1066. https://doi.org/10.11817/j.issn.1672-7347.2025.240688.
CAO Saiying, LONG Yi, YANG Lina. Research progress in the role of caspase-3 in regulating pyroptosis and apoptosis in non-alcoholic fatty liver disease[J]. Journal of Central South University. Medical Science, 2025, 50(6): 1060-1066. https://doi.org/10.11817/j.issn.1672-7347.2025.240688.

[42] Xu G, Wei S, Yu C, et al. Activation of Kupffer cells in NAFLD and NASH: mechanisms and therapeutic interventions [J]. Front Cell Dev Biol, 2023, 11: 1199519. https://doi.org/10.3389/fcell.2023.1199519.

[43] Bonnardel J, Jonck W, Gaublomme D, et al. Stellate cells, hepatocytes, and endothelial cells imprint the kupffer cell identity on monocytes colonizing the liver macrophage niche [J]. Immunity, 2019, 51(4): 638-654. https://doi. org/10.1016/j.immuni.2019.08.017.

[44] Wandrer F, Liebig S, Marhenke S, et al. TNF-Receptor-1 inhibition reduces liver steatosis, hepatocellular injury and fibrosis in NAFLD mice[J]. Cell Death Dis, 2020, 11(3): 212. https://doi.org/10.1038/s41419-020-2411-6.

[45] Gao X, Xu X, Belmadani S, et al. TNF-alpha contributes to endothelial dysfunction by upregulating arginase in ischemia/reperfusion injury[J]. Arterioscler Thromb Vasc Biol, 2007, 27(6): 1269-1275. https://doi.org/10.1161/ATVBAHA.107.142521.

[46] Gan C, Yaqoob U, Lu J, et al. Liver sinusoidal endothelial cells contribute to portal hypertension through collagen type IV-driven sinusoidal remodeling[J/OL]. JCI Insight, 2024, 9(11): e174775[2026-02-01]. https://doi. org/10.1172/jci. insight.174775.

[47] Gibert-Ramos A, Sanfeliu-Redondo D, Aristu-Zabalza P, et al. The hepatic sinusoid in chronic liver disease: the optimal milieu for cancer[J]. Cancers, 2021, 13(22): 5719. https://doi.org/10.3390/cancers13225719.

[48] DeLeve LD. Liver sinusoidal endothelial cells and liver regeneration[J]. J Clin Invest, 2013, 123(5): 1861-1866. https://doi.org/10.1172/JCI66025.

[49] Lu S, Wang Y, Liu J. Tumor necrosis factor-α signaling in nonalcoholic steatohepatitis and targeted therapies[J]. J Genet Genom, 2022, 49(4): 269-278. https://doi.org/10.1016/j.jgg.2021.09.009.

（责任编辑 田朴）

©Journal of Central South University (Medical Science). All rights reserved.